Available online at www.sciencedirect.com
SCIENCE DIRECT
Catalysis Today 109 (2005) 24–32
CATALYSIS TODAY
www.elsevier.com/locate/cattod

A comparative study for heavy oil hydroprocessing catalysts at micro-flow and bench-scale reactors

Mohan S. Rana *, J. Ancheyta, P. Rayo

Instituto Mexicano del Petróleo, Eje Central Lázaro Cárdenas 152, Mexico D.F. 07730, México

Available online 10 October 2005

Abstract

CoMo and NiMo catalysts were prepared and the catalytic activities were evaluated in fixed bed micro-flow and bench-scale reactors with different feed composition. Experiments were conducted at conditions close to those that exist in the industrial practice. Due to the different nature of the feeds, the conditions were varied with respect to both evaluation scales. The fresh and spent catalysts were characterized. Spent catalyst textural properties indicated that catalysts were deactivated and the surface area and pore volume dropped by 20–60%. The adsorption–desorption hysteresis of spent catalysts indicated that cylindrical pores are deactivated at the pore mouth and played an important role in modification by either closing one end of the pore or forming a narrow neck pore, which is indicative of the formation of "*ink-bottle*" type pores. Thus, the deposition of metal and carbon takes place preferentially at the pore entrance, which causes pore mouth plugging. These results are also supported by the SEM–EDAX analysis, where metal and carbon depositions are evident and taking place at the superficial region of a catalyst particle. The increase in absolute area of hysteresis is based on the catalyst's average pore diameter: the higher the average pore diameter, the lower the area of the spent catalyst. The activity and deactivation of the catalyst are discussed on the basis of catalyst porosity and deposited metal characterization. The composition of catalysts varies, considering two applications in a multi-reactor system: a CoMo catalyst for the first reactor, and a NiMo in the second reactor; the former is supported on γ-Al_2O_3 and the latter on TiO_2/Al_2O_3. As a comparison, the CoMo catalyst exhibited better hydrogenolysis while the NiMo catalyst showed better hydrogenation activity in both micro-flow and bench-scale reactors. It appears that there is a moderate effect of TiO_2 content in support on Ni and V hydrodemetallization (HDM) while hydrodeasphaltenization (HDAs) and hydrodesulfurization (HDS) activities were slightly improved when a partially hydrotreated feed, which contains more refractory compounds than virgin feedstock, was employed.

Keywords: HDM; HDS; HDAs; Metal deposition; Spent catalysts; Maya crude; Micro-flow and bench-scale reactors; SEM–EDAX; Deactivation

1. Introduction

The tightening of environmental legislation on transportation fuel quality is being implemented or planned throughout the world [1,2]. Since the quality of petroleum feed, its configuration, and the complexity of refinery processes can vary substantially, each refinery has its own strategy to meet the new goals of fuel specification. Each country develops new product specifications, but the implementation time for these new specifications varies, depending on the region and origin of fuel oils. In some countries, as in the case of Japan since 2003, the refiners have started marketing and distributing less than 50 wppm sulfur gas oil ahead of legislation [3]. Looking at the trend, the demand for middle distillates has been growing day by day. However, heavy oils fraction contains high amounts of sulfur and other contaminants that exhibit different reactivity during hydroprocessing, and depending on their complexity, can affect the course of reactions differently; to the point that they can even deactivate the catalyst at a very fast rate. Therefore, before hydroprocessing heavy oil, there are two main concerns that need to be considered: (i) environmental specification; and (ii) product selectivity. In the first case, the presence of the so-called refractory compounds means difficult hydrodesulfurization, complicating the production of ultra-low sulfur fuels. The second case involves the different functionalities of the hydrotreating catalyst, i.e. hydrogenolysis, hydrogenation, and hydrocracking, which can also have an impact on the final product quality depending on both feed and catalyst compositions. Thus, to satisfy both concerns, upgrading of heavy oil is mandatory. On the other hand, refiners are

* Corresponding author. Tel.: +52 55 9175 8418; fax: +52 55 9175 8429.
E-mail address: msingh@imp.mx (M.S. Rana).

0920-5861/$ – see front matter © 2005 Elsevier B.V. All rights reserved.
doi:10.1016/j.cattod.2005.08.008

facing a dilemma in trying to keep oil prices more or less steady in spite of treating the crude with more expensive processing methods. For instance, in Mexico, the major refining facilities are located along the Gulf of Mexico under the brand name of PEMEX (Mexican oil company), and the refineries require next generation hydrotreating catalysts due to the high production of heavy crudes which need to be processed. Similarly, other countries like Venezuela, Canada, etc. are facing the same kind of problems.

Keeping in mind the aforementioned concerns, the Mexican Institute of Petroleum is working on upgrading heavy oils through the hydroprocessing of Maya crude. Sometimes dilution of heavy crude with light feedstocks is necessary to minimize the experimental problems occurring due to high viscosity of the Maya crude. Rayo et al. [4] reported a detailed study of the diluent effect on Maya crude hydrotreating. The prime target of heavy oil processing is to develop an HDM catalyst and to protect downstream HDS, HDA, and HDN catalysts, which are loaded in the second reactor of a multi-reactor system. Usually, the HDM catalysts are loaded in the first reactor as a guard [5]. With respect to feed composition, vanadium is mainly concentrated in heavy fractions as vanadyl porphyrins and is associated with other large molecules containing condensed poly-aromatic rings [6]. Therefore, the pore structure of HDM catalysts should be designed to handle these metal compounds of large molecular size. In general the HDM catalyst (first reactor) is designed with high porosity and low surface area [7], while the HDM/HDS catalyst (second reactor) is characterized by higher surface area and moderate pore size distribution. Apart from this, the large pore catalysts enhance diffusion of asphaltene into the interior of the catalyst and provide a larger pore to accommodate metal deposits. On the other hand, the mixed oxide supported catalysts are slightly more acidic than pure alumina, which favors the deep desulfurization and enhances the hydrocracking [8]. Now, it is clear that in order to develop a suitable heavy oil hydrotreating catalyst, large pore diameter is of primary importance, while the nature and/or dispersion of active sites is secondary, which is the exact opposite of any other hydrotreating catalysts [9,10].

The major goal of the present study is to compare the behavior of catalysts for Maya crude hydrotreating with adequate stability with time-on-stream on two evaluation scales: micro-flow and bench-scale reactors. The comparison is made considering a CoMo catalyst with high porosity (HDM) and a NiMo catalyst which will be more prone to the deep HDS (HDS/HDM) using, respectively, Al_2O_3 and TiO_2/Al_2O_3 as support. The activity tests were carried out at conditions close to those that exist in the industrial practice. Stability or catalyst deactivation after 120 and 200 h (TOS) was followed by monitoring the changes in conversion, product quality, and in the textural properties of spent catalysts, which indicate that metal deposition takes place at the pore mouth. The deposition of metal is also confirmed by the scanning electron microscopy–energy dispersion analysis by X-ray (SEM–EDAX) analysis. Studies were undertaken to determine the relationship between hydrodemetallization performances, catalytic pore diameter, and pore structure.

2. Experimental

Pure alumina support was prepared by using the *urea hydrolysis* homogeneous precipitation method, employing aluminum nitrate solution (∼1.5 M) and a sufficient amount of urea [10]. The solution was refluxed at about 95 °C (±3 °C) for 10 h (controlling the pH of precipitate at ≈7.5–8.5), to allow the precipitation of aluminum hydroxides. The milky white precipitate appears during the refluxing at the aforementioned temperature. The precipitate was aged overnight (10 h), filtered, and washed. The wet extrudate was prepared from precipitate and dried overnight at 120 °C. The γ-Al_2O_3 sample is represented as pure alumina (PA).

The dry extrudate of boehmite support prepared using 2.5% (v/v) HNO_3 for peptization of alumina and titanium isopropoxide was impregnated using the incipient wetness method over 550 °C calcined extrudate. The TiO_2 impregnated extrudates were calcined at 450 °C. The TiO_2/Al_2O_3 sample is labeled as TA support.

The molybdenum-supported catalysts were prepared by the incipient wetness impregnation method. An appropriate amount of ammonium heptamolybdate (AHM) (Fluka AR grade) was used and dissolved in ammoniac solution. The Co and Ni-promoted catalysts were also prepared via the sequential impregnation procedure on Mo-loaded catalysts (dried at 120 °C and calcined at 400 °C). The cobalt and nickel nitrate salts were impregnated in an aqueous medium. The final catalysts were dried in presence of air at 120 °C overnight and calcined at 450 °C for 4 h. The compositions of support and supported catalysts are reported in Table 1.

Table 1
Composition of support and catalyst

Sample	Support			Catalyst		
	Composition	Textural properties		Ni	Co	Mo
		SSA (m^2/g)	PV (ml/g)			
CoMo/PA-MFR	Al_2O_3	184	0.481	–	2.10	5.93
CoMo/PA-BSR	Al_2O_3	–	–	–	2.10	5.93
NiMo/AT-MFR	5 wt.% TiO_2/Al_2O_3	176	0.402	4.12		6.56
NiMo/AT-BSR	5 wt.% TiO_2/Al_2O_3	–	–	4.12		6.56

PA (pure γ-Al_2O_3); TA (TiO_2/Al_2O_3); MFR (catalyst tested in micro-flow reactor); BSR (catalyst tested in bench-scale reactor).

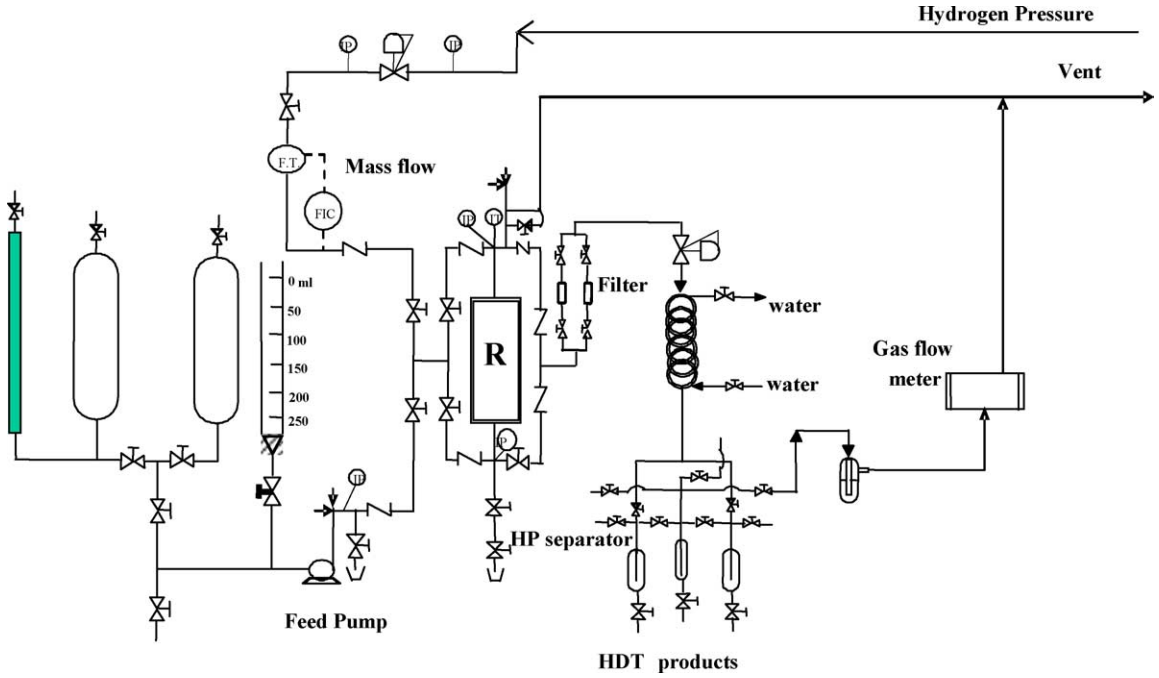

Scheme 1. Flow diagram of fixed bed up flow micro-flow reactor.

The BET specific surface area (SSA), pore volume (PV), and pore size distribution (PSD) were carried out in Quantochrome Nova 2000 equipment. Nitrogen gas was employed for SSA measurements at liquid nitrogen temperature (−196 °C). Prior to the adsorption, the samples were degassed for 3 h at 300 °C.

Pyridine probe molecule was used for FT-IR spectroscopic studies to distinguish the acidity of supported catalysts. Catalysts were sulfided at 400 °C for 2 h before probe molecule adsorption. Adsorptions of probe molecules were carried out at room temperature. The pyridine adsorbed samples were heated at different temperatures; consequently, changes in acidity could be observed as a function of temperature.

To evaluate the catalytic behavior with real feed, the catalysts were tested in a high pressure micro-flow reactor and in a bench-scale reactor as shown in Schemes 1 and 2. The properties of the different feedstock for each plant are presented

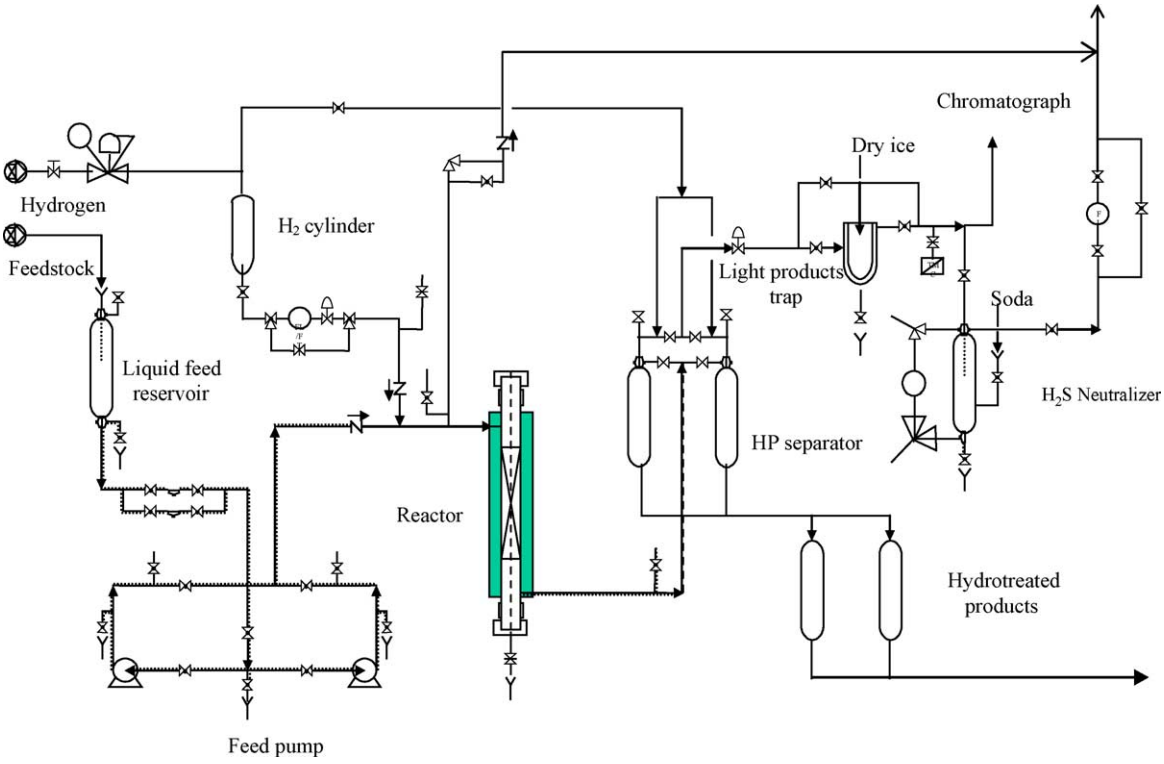

Scheme 2. Flow diagram of fixed bed down flow bench-scale reactor.

Table 2
Physico-chemical characterization of feed for different reactors

Properties	Bench-scale reactor feed		Micro-flow reactor feed	
	Maya crude	Maya HDT	HDM[a]	HDS[b]
Elemental analysis (wt.%)				
C	86.9	85.5	84.2	83.2
H	5.3	7.2	8.8	9.5
N	0.3	0.1852	0.184	0.118
S	3.52	1.217	2.21	0.648
Metal (wpm)				
Ni	49.5	36.76	26.21	18.9
V	273.0	107.98	124.78	81.66
(Ni + V)	322.5	144.74	150.99	100.56
Ca	11.26	–	5.0	–
Mg	2.04	–	1.01	–
Na	44.83	–	21.2	–
K	20.25	–	10.2	–
Fe	2.16	–	1.02	–
Asphaltene, wt.% (n-C_7 in sol.)	12.7	6.87	8.43	–
Physical properties				
Density (20/4 °C)	0.925	0.877	0.88	0.865
Pour point (°C)	−30	–	−15	−24
Ramscarbon (wt.%)	10.87	8.0	5.45	5.54
API gravity	21.31	31.14	29.29	32.10
Viscosity (g/cm s)				
at 50 °C	–	–	3.08	2.63
at 100 °C	–	–	9.45	8.29

Maya HDT (Maya hydrotreated partially).
[a] HDM feed (Maya + diesel, 50/50 (w/w)).
[b] HDS feed (Maya HDT + diesel, 50/50 (w/w)).

in Table 2. The post-HDM Maya crude with diesel is named HDS feedstock and pure Maya crude with diesel is known as HDM feed.

The catalyst pretreatment and the hydrotreating reactions were both carried out in high-pressure integral fixed-bed reactors. The reactor was loaded with an oxidic catalyst with 3–5 mm extrudate size diluted with an equal volume of SiC. The catalyst was sulfided in situ using a mixture of dimethyldisulfide (DMDS), straight run gas oil (SRGO), and H_2. After depressurizing the reactor to atmospheric pressure, the sulfiding feed (1 wt.% DMDS + SRGO) containing ≈2.0 wt.% ''S'' was started in order to wet the catalyst bed at room temperature. The liquid was drained after 4 h, and then the temperature rose linearly from 30 to 120 °C (30 °C/h) and remained as such for 2 h. Later, the temperature was increased at the rate of 30 °C/h until it reached 150 °C, at 2.8 MPa pressure and remained as such for 2 h. The temperature was further increased to 260 °C and remained as such for 3 h. The final temperature of sulfidation was 320 °C, which was stabilized for 5 h at 2.8 MPa. After sulfidation, the flow was switched to the corresponding feed and the operating conditions were adjusted as shown in Table 3. The process conditions used are typical for Maya crude processing of reactions with moderate severity. These conditions were selected based on the literature as well as on our own experience working with the Maya crude.

Metals (Ni, V) were analyzed in the feed and products using flame atomic absorption spectrometry (ASTM D 5863–00a method). The total S content was analyzed with the HORIBA model SLFA-2100/2800, using scattered spectroscopy by sulfur, generating energy dispersive X-ray fluorescence. The X-ray beam was separated selectively with the help of a filter and detected as sulfur concentration. Nitrogen was measured by oxidative combustion and chemiluminescence (ASTM D 4629-02 method) at high temperature combustion in an oxygen rich

Table 3
Reaction conditions for fixed-bed integral reactors

Conditions	Micro-flow reactor	Bench-scale reactor
Temperature (°C)	380	400
Pressure (MPa)	5.4	7.0
Hydrogen flow (L/h)	4.6	90
Flow of Maya crude (mL/h)	10	100
LHSV (h^{-1})	1.0	1.0
Hydrogen/oil ratio (m^3/m^3)	356	891.0
Mode of operation	Up flow	Down flow
Time-on-stream (h)	120	200
Catalyst volume, mL (g)	10 (8.5)	100 (85.0)
Catalyst shape	Cylindrical extrudate	Cylindrical extrudate
Catalyst size (in.)	1/16	1/16
Feed composition tested		
Pure Maya crude	–	√
Maya HDT	–	√
HDM feed	√	–
HDS feed	√	–

atmosphere. Asphaltene is defined as the insoluble fraction in *n*-heptane, which is an indirect measure of dry-sludge formation. The solid carbonaceous material on spent catalysts (toluene washed) was analyzed with a Leco SC-444 instrument using ASTM C 1408-98 method by direct combustion-infrared detection.

The surface morphology of catalysts was studied by means of elemental analysis with the SEM–EDAX analytical instrument xT Nova NanoLab 200 (FEI Schottky FEG, 30–1 keV), combined with a dual high resolution focused ion beam (Ga FIB) using detector type SUTW, Sapphire with LEAP + - crystals for the best light element performance of the Si(Li) detector. The sample was deposited on a carbon holder and evacuated at high vacuum (10^{-5} Torr) before images were taken. Five representative analyses were taken to confirm the results. The analysis was made across the radial line of the extrudate; five points were chosen, e.g. external, semi-external, center, and vice-versa.

3. Results and discussion

3.1. Catalytic activities

The catalytic activities were studied for two different catalysts (CoMo and NiMo) in micro-flow and bench-scale reactors using different feedstocks (Table 2). The composition of the feedstock such as metal, sulfur, nitrogen, and asphaltenes varies in the different plants. This difference in the feed composition may have a considerable effect on catalyst performance [4]. However, the variation of feed in the different plants is necessary to minimize the experimental problems, due to the low viscosity or low API gravity of Maya crude, generated during the course of feed processing.

3.1.1. Micro-flow reactor (MFR)

Fig. 1 shows the results of the activity behavior on the $CoMo/Al_2O_3$ catalyst at micro-flow evaluation scale using HDM feed (50% Maya and 50% diesel) for HDS, HDM, and HDAs reactions against time-on-stream (TOS). The catalytic results indicate that this catalyst is more active for hydrogenolysis than hydrogenation of asphaltenes. The catalyst stability against TOS is more or less the same for HDS and HDM, while HDAs activity decreases slightly with a faster rate, which could be due to the diffusion of complex asphaltene molecules into the pores, or to the higher acidity of the catalyst. The lower HDAs activity is a well-known fact for the CoMo catalyst which possesses less of the hydrogenation than of the hydrogenolysis function.

On the other hand, the $NiMo/TiO_2/Al_2O_3$ (TA) catalyst activity is shown in Fig. 2 using HDS feed, which contains less sulfur, metal (Ni + V), and asphaltenes than HDM feed (Table 2), but the nature of these molecules differs owing to the fact that in the case of HDS feed more refractive sulfur will be expected. Fig. 2 indicates that there is no distinguishable difference between the three conversions, especially after 100 h TOS. We could not observe clearly the role of TiO_2 in support in comparison to the pure alumina supported catalyst. The reason

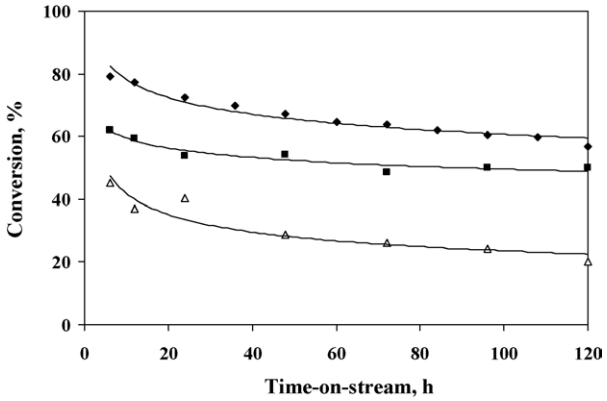

Fig. 1. Catalytic activity in micro-flow reactor with time-on-stream over $CoMo/\gamma\text{-}Al_2O_3$ catalysts against HDM feed: (◆) HDS; (■) HDM; (△) HDAs.

for this might be the different nature of feedstock considering all catalytic activities remain lower except for hydrodearomatization (HDAs) of asphaltenes, which must be due to the role of Ni.

It is well-known that crude oil contains various sulfur compounds with different reactivity [11,12]; hence, the relatively more refractory sulfur compounds are expected to appear in HDS feedstock rather than HDM feedstock. In the case of the former, due to its previous treatment, most of the easier to desulfurize sulfur compounds have already been removed. Sixty percent HDS conversion is achieved when using HDM feed, and then it is most likely that HDS feedstock has more than 75% refractory sulfur compounds. Thus, it appears from these results that NiMo is not only increasing asphaltenes hydrogenation, but also having an inducing effect on the aromatic ring structure hydrogenation so that cleavage of the ring structure takes place and is followed by the removal of sulfur from refractory compounds. Of course, this observation must be supported by the detailed analysis of refractory compounds, which is almost impossible due to the complexity of Maya crude; nevertheless, product distillation results and its gas chromatography analysis helps elucidate the imaginary composition of sulfur [13]. On the other hand, the effect of pore

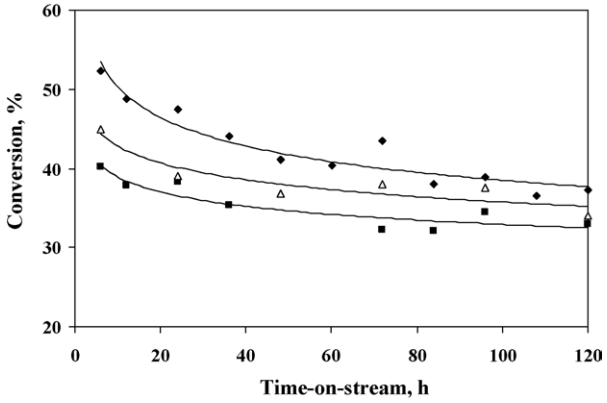

Fig. 2. Catalytic activity in micro-flow reactor with time-on-stream over $NiMo/TiO_2/Al_2O_3$ catalysts against HDS feed: (◆) HDS; (■) HDM; (△) HDAs.

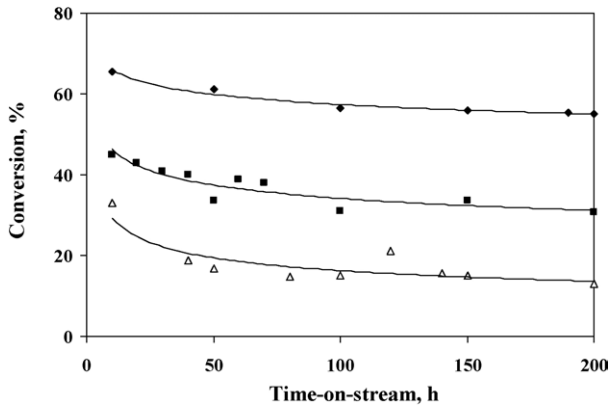

Fig. 3. Catalytic activities on bench-scale reactor (CoMo/γ-Al_2O_3) with time-on-stream: (◆) HDS; (■) HDM; (△) HDAs.

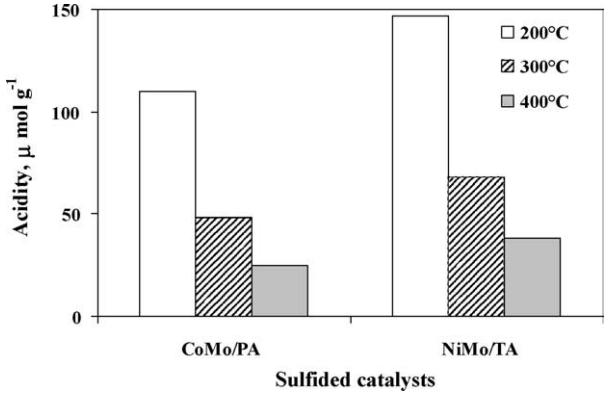

Fig. 5. Lewis acidity of sulfided catalysts as an effect of support composition.

size distribution may also play a role, but the impact of porosity on diluted Maya crude should be less than on pure crude.

3.1.2. Bench-scale reactor (BSR)

Considering the stability of catalysts on the micro-flow scale, the same catalysts were tested against pure Maya crude and partially hydrotreated Maya crude (Maya HDT). The results for different activities against TOS are shown in Figs. 3 and 4 for CoMo and NiMo catalysts, respectively. Fig. 3 shows that all activities marginally decrease with TOS. As expected, the CoMo catalyst showed much lower activity for the hydrogenation of asphaltenes than HDM and HDS activities. However, the decay in activity with time-on-stream for the three reactions is very similar, which indicates that the catalytic sites remain constant or vary similarly with time for all catalytic activities. Surprisingly, we observed a more or less similar deactivation trend for the micro-flow reactor as well as the bench-scale reactor, while the compositions of feedstocks were entirely different (Table 2). This consistence of activity with time-on-stream could be related to the porosity of the catalyst, which for hydrotreating of heavy oil is directly proportional to the stability of the catalysts [10]. On the other hand, the stability of the NiMo catalyst (Fig. 4) is not similar for all activities, e.g. the conversion of HDAs decreases faster than HDS and HDM.

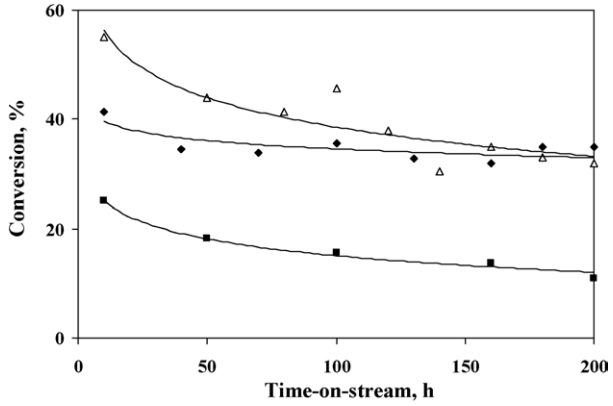

Fig. 4. Catalytic activities on bench-scale reactor (NiMo/TiO_2/Al_2O_3) with time-on-stream: (◆) HDS; (■) HDM; (△) HDAs.

Obviously, in this case HDAs activity is higher than HDS and HDM, which further revealed that the NiMo catalyst enhances the hydrogenation of asphaltenes. The odd deactivation for HDAs in the case of NiMo/TA indicated a role of catalyst acidity, which is higher in the case of the NiMo/TA supported catalyst as shown in the Fig. 5, and may, to some extent, play a role in cracking asphaltene molecules. However, the differences between the two catalysts are small, but they appear to be sufficient to explain the behavior of catalysts. Nevertheless, the sulfided catalysts showed a negligible amount of Brönsted acidity at 1541 cm^{-1} after 200 °C desorption. On the other hand, a sufficient number of Lewis acid sites remains up to 400 °C. The IR bands at 1598 and 1445 cm^{-1} are specific to pyridine interaction with the Lewis acid sites and quantification of these bands is shown in Fig. 5.

Thus, the faster deactivation on the hydrogenation route may be due to some acidic sites generated by the mixing of TiO_2 and Al_2O_3, which favors the cracking of asphaltene molecules and the subsequent deactivation by coke deposition. One more plausible explanation with this respect is the stability for HDS and HDM activities with TOS, which indicates that the metallic site (coordinative unsaturated site) in the hydrotreating catalyst is more stable than the acidic site of support or active phases (–SH groups) [14,15]. However, the catalyst deactivation with heavy oil processing is not only due to the carbon deposition, it is equally possible that metallic sites (Co–Mo–S) have been poisoned by Ni and V deposition during the HDM, although surely the cracking site will be deactivated faster than the metallic site. The deposition of metals or carbon is most likely at the entrance of the pore or on the surface, which plugs the pore mouth or restricts diffusion of big, complex asphaltene molecules into the pores [9].

A comparison of conversions between the two different reactors for the same catalyst after 120 h TOS is shown in Table 4. Again, the composition of the feeds with each catalyst is not the same, but the nature of the active site can be predicted and the effect of porosity can be represented, which results in a lower chance of pore mouth plugging that accelerates diffusion of metal compounds; thus, metal is eventually deposited throughout the catalyst surface [16–18]. The hydrogenolysis

Table 4
Comparison between micro-flow and bench-scale activities data after 120 h TOS

Catalysts	Conversion (%)		
	HDS	HDM	HDAs
CoMo/PA-MFR	56.6	50.0	40.0
CoMo/PA-BSR	56.6	31.2	14.9
NiMo/TA-MFR	37.3	35.4	34.0
NiMo/TA-BSR	35.6	15.7	45.7

selectivity (HDM versus HDS) of both catalysts (CoMo and NiMo) followed a similar tendency as shown in Fig. 6a. A relationship between HDM and HDS conversions for different catalysts indicates that both hydrogenolysis activities C–M and C–S bond breakages involve the same kind of site, and it seems that there are no diffusion limitations against the HDS molecule due to the pore size distribution. On the other side, HDM selectivity is plotted against the HDAs and shown in Fig. 6b in which it is clearly observed that the CoMo catalyst is selectively good for HDM and NiMo is better for HDAs. The explanation for this is that NiMo is widely known to be a hydrogenation catalyst, while the CoMo catalyst porosity may play an important role in distinguishing the two different functionalities.

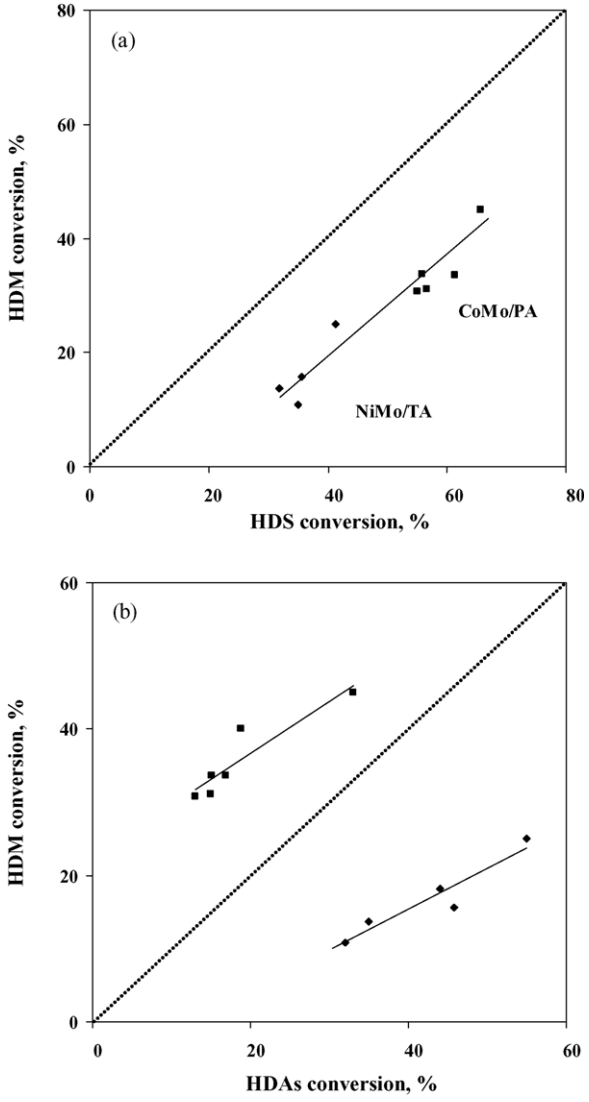

Fig. 6. Different catalysts (■ CoMo/PA; ◆ NiMo/TA) selectivities in bench-scale reactor: (a) HDM selectivity against HDS; (b) HDM selectivity against HDAs.

3.2. Textural properties of fresh and spent catalysts

A common concern in heavy oil processing is the avoidance of pore blockage due to metal and carbon accumulation at the pore mouth, in other words, metal retention capacity with time-on-stream. Thus, in this work, detailed studies were undertaken to determine the relationship among the activity performance and catalyst textural properties such as total pore volume, average pore diameter, and adsorption–desorption isotherms. The fresh and spent catalyst textural properties are given in Table 5. From these results, it is clear that deposition of metals and coke alters the nature and/or the number of pores. The spent catalyst SSA and total pore volume decrease by 20–30% and 55–60%, respectively, in the case of CoMo, while for the NiMo catalyst, SSA and total pore volume are reduced by 28–35% and 40–45%, respectively. Pore volume and surface area of the catalyst used in the bench-scale reactor decrease slightly more in both cases than micro-flow reactor catalysts due to the severity of process conditions as well as feedstock composition.

With respect to the aforementioned arguments, it appears that most of the metal (Ni + V) and coke are deposited near the pore mouth, which changes the cylindrical pores into the ''*ink-bottle*'' type of pores; similar results are reported in our pervious work [9]. These deposits may cover the active catalyst site and cause pore constriction for the diffusion of reactant molecules. The predictions of pore constriction were reported in the literature, but we tried to prove them experimentally by using nitrogen adsorption–desorption hysteresis loop area. The relative adsorption–desorption isotherms of fresh and spent catalysts are shown in Figs. 7 and 8 for CoMo and NiMo catalysts. The corresponding absolute areas of the isotherm were calculated using the trapezoidal rule integration method and are reported in Table 6. These results also revealed that the pores are not completely blocked [19,20], though they may be blocked for reactant molecules but not for the N_2 adsorption–desorption; however, this will depend on the catalyst pore size and time-on-stream. Now a question is still unanswered: why does the isotherm area increase in the case of spent catalysts?

Table 5
Textural properties of fresh and spent catalysts

Catalysts	Fresh catalysts			Spent catalysts		
	SSA	PV	APD	SSA	PV	APD
CoMo/PA-MFR	153.2	0.4378	10.0	120.3	0.1947	6.5
CoMo/PA-BSR	153.2	0.4378	10.0	109.5	0.1969	7.2
NiMo/TA-MFR	166.7	0.3071	7.3	120.2	0.1707	5.7
NiMo/TA-BSR	166.7	0.3071	7.3	111.2	0.1763	6.3

SSA, specific surface area (m^2/g); PV, pore volume (ml/g); APD, average pore diameter (nm).

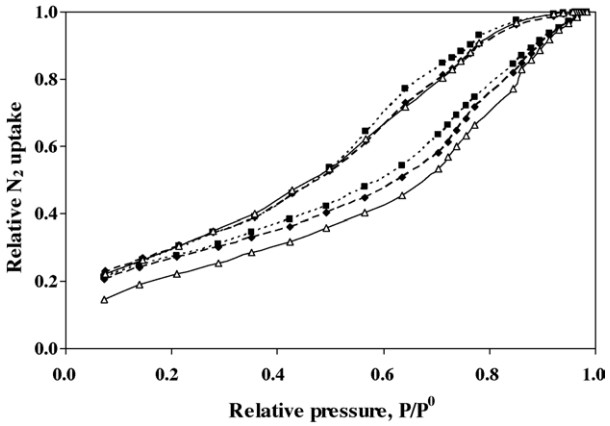

Fig. 7. Fresh and spent catalysts (CoMo/PA) adsorption–desorption isotherms: (■) fresh catalyst; (◆) spent catalyst-MFR; (△) spent catalyst-BSR.

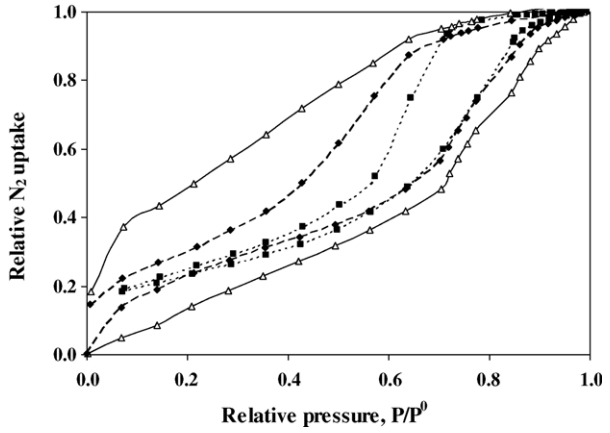

Fig. 8. Fresh and spent catalysts (NiMo/TA) adsorption–desorption isotherms: (■) fresh catalyst; (◆) spent catalyst-MFR; (△) spent catalyst-BSR.

Any answer to this question calls for a discussion regarding the origin of hysteresis. One possibility is that the nature of the pore in the actual model of pore shape (cylindrical) is altered by metal deposition at the pore mouth, and as a result, the physic-sorbed nitrogen in "*ink-bottle*" pores (most probably N_2 in condensed phase) cannot be desorbed until the relative pressure is low enough [9]. This results in an increase in the isotherm area. These results are complementary to the spent catalyst analysis by atomic absorption in Table 7. The quantitative distribution of carbon, V, and Fe shows maximum concentrations on the CoMo bench-scale reactor catalyst. The deposition of carbon and Fe on the CoMo bench-scale reactor catalyst is almost double that found on the CoMo micro-flow catalyst, and it still maintains good stability for HDS and HDM activities with time-on-stream. Therefore, the metal retention capacity

Table 6
Fresh and spent catalysts N_2 adsorption–desorption hysteresis loop area

Catalysts	Fresh catalyst	Spent catalyst	
		Micro-flow reactor	Bench-scale reactor
Expected nature of pores	Cylindrical	Ink-bottle	Ink-bottle
CoMo/PA	0.0865	0.101	0.139
NiMo/TA	0.0685	0.164	0.338

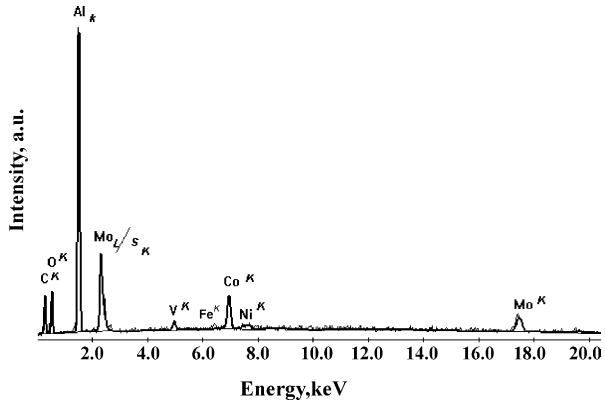

Fig. 9. Micro analysis of elemental composition of spent catalyst (CoMo/PA) using SEM–EDAX.

increases as the pore diameter of the catalyst increases, and it has better stability or a longer life span.

3.3. Elementary analysis of spent catalysts: SEM–EDAX

Elementary analysis of spent catalysts is carried out by using SEM–EDAX indicating that vanadium and nickel are present as metal sulfides, most probably V_2S_3 and Ni_3S_2. We have demonstrated this before by using the spent catalyst XRD [10]. The qualitative analysis of deposited metal and carbon on the surface of the CoMo/Al_2O_3 spent catalyst is shown in Fig. 9. Since most of the metalloporhyrins are associated with the asphaltene molecules, it is plausible that some of the asphaltene molecules do not diffuse into the catalyst. Consequently, their conversion took place at the entrance to the pore mouth due to pore diffusion limitation. Furthermore, these results are confirmed by quantitative analysis of V metal as a function of extrudate radial distribution zones, which shows an enrichment of V and Ni in the superficial region of the catalyst particle. The deposition of intra-particle vanadium metal profile is shown in Fig. 10. Similar results on the used catalysts were reported by Audibert and Duhaut [21] and Radford and Rigg

Table 7
Analyses of spent catalysts (wt.%)

Catalysts	Mo	Co	Ni	V	C	S	Fe (wppm)	S/Mo (mol/mol)
CoMo/PA-MFR	4.711	1.543	0.140	0.558	8.66	5.10	201.5	3.25
CoMo/PA-BSR	4.301	1.45	0.302	1.393	13.3	3.81	804.5	2.66
NiMo/TA-MFR	4.867	–	3.860	0.061	7.10	4.42	176.4	2.72
NiMo/TA-BSR	3.860	–	3.860	0.171	7.53	4.30	320.1	3.34

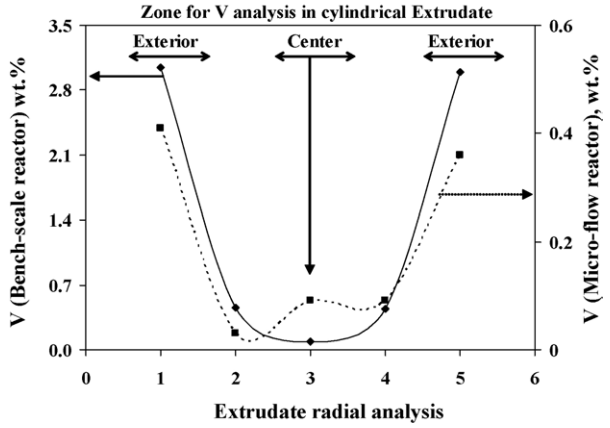

Fig. 10. Deposited metal concentration profiles obtained by SEM–EDAX on the micro-flow and bench-scale reactors (radial distribution of vanadium).

[22], who found higher concentration of deposited metal at the outer surface compared with the inner surface. In a comparison between two different reactors ($CoMo/Al_2O_3$), one can also notice the intensities of V radiation in that the bench-scale reactor showed almost five–six times higher deposition than the micro-flow reactor catalyst. The deposition of metal depends on the composition of feedstock as well as reaction conditions (Tables 2 and 3). Moreover, the SEM–EDAX results are complementary to the isotherm area calculated (Table 6) by using N_2 adsorption–desorption. The metal concentration in Fig. 10 was in the pellet, and it measures the metal retention capacity of the catalyst, and thus, the life of catalyst. Therefore, even with EDAX results, the accumulation of metal sulfide remains qualitative or speculative regarding pore mouth plugging; however, the isotherm area can include a semi-quantitative manner of calculating the deposition of metal and carbon at the pore mouth.

4. Conclusions

Urea hydrolysis prepared support provides macro-porous material. The incorporation of TiO_2 into the support may help to increase the number of catalytic sites as well as the acidity of support which enhances the cracking of hydrogenated asphaltenes. The effect of pore diameter appears more important than the number of catalytic sites or active phases for heavy oil hydroprocessing catalysts. The spent catalysts drop specific surface area by 20–40%, and total pore volume by 40–60%, due to the deposited metal, carbon, and sulfur on the surface, which is so high that it can overlap the fresh catalyst active phases ($Co–MoS_2$) and restrict the diffusion of reactants to the active sites. Therefore, deposited metal and coke decrease catalyst conversion due to the diffusion of reactant molecules into the pores by wage type deposited at the pore mouth. The pore mouth plugging was confirmed by calculating the hysteresis area, which can be a semi-quantitative manner of determining catalyst deactivation at the pore mouth: area increases with the increasing deactivation of the catalyst. An increase in hysteresis loop area and SEM–EDAX results confirm that due to the severity of reaction conditions and the nature of feedstock, the catalysts used in the bench-scale reactor are comparatively more deactivated than those employed in the micro-flow reactor.

Acknowledgements

The authors thank I.M.P. for financial support. We express our appreciation to Mr. José G. Espinosa and Mrs. Bertha Núñez for helping with the preparation of feeds and adsorption–desorption experiments.

References

[1] Y. Okamoto, M. Breysse, G. Murali Dhar, C. Song, Catal. Today 86 (2003) 1.
[2] H. Topsøe, B.S. Clausen, F.E. Massoth, in: J.R. Anderson, M. Boudart (Eds.), Hydrotreating Catalysis—Science and Technology, Vol. 11, Springer–Verlag, New York, 1996.
[3] S. Fukase, S. Akashah, Hydrocarbon Asia, March/April (2004) 24.
[4] P. Rayo, J. Ancheyta, J. Ramirez, A. Gutierez-Alejandre, Catal. Today 98 (2004) 171.
[5] J.W. Gosselink, CatTech 2 (1998) 127.
[6] J.F. Le Page, J. Cosyns, P. Courty, E. Freund, J.-P. Franck, Y. Jscquin, B. Juguin, C. Marcilly, G. Martino, J. Miquel, R. Miquel, R. Montarnal, A. Sugier, H. Van Landeghem (Eds.), Applied Heterogeneous Catalysis, Design, Manufacture, Use of Solid Catalysts, Technip, Paris, 1987.
[7] H. Toulhoat, R. Szymanski, J.C. Plumail, Catal. Today 7 (1990) 531.
[8] S.K. Maity, J. Ancheyta, L. Soberanis, F. Alonso, Appl. Catal. A 250 (2003) 231.
[9] M.S. Rana, J. Ancheyta, S.K. Maity, P. Rayo, Catal. Today 104 (2005) 86.
[10] M.S. Rana, J. Ancheyta, P. Rayo, S.K. Maity, Catal. Today 98 (2004) 151.
[11] F. Bataille, J.-L. Lemberton, P. Michaud, G. Perot, M. Vrinat, M. Lemaire, E. Schulz, M. Breysse, S. Kasztelan, J. Catal. 191 (2000) 409.
[12] T. Isoda, S. Nagaro, X. Ma, Y. Korai, I. Mochida, Energy Fuels 10 (1996) 1078.
[13] J. Ancheyta, unpublished results.
[14] M. Rana, S.K. Maity, J. Ancheyta, G. Murali Dhar, T.S.R. Prasada Rao, Appl. Catal. A 258 (2004) 215.
[15] M.S. Rana, R. Navarro, J. Leglise, Catal. Today 98 (2004) 67.
[16] E. Furimsky, F.E. Massoth, Catal. Today 52 (1999) 381.
[17] J. Bartholdy, B.H. Cooper, in: M. Absi-Halabi, et al. (Eds.), Catalyst in Petroleum Refining and Petrochemical Industries, Elsevier, Amsterdam, 1995, p. 117.
[18] M. Marafi, A. Stanislaus, Appl. Catal. A 159 (1997) 259.
[19] T.H. Fleisch, B.L. Meyers, J.B. Hall, G.L. Ott, J. Catal. 86 (1984) 147.
[20] B.J. Johnson, F.E. Massoth, J. Bartholdy, AIChE J. 32 (1986) 1980.
[21] F. Audibert, P. Duhaut, Rev. de l'Institut Francais du Pétrole 25 (5) (1970) 613.
[22] H.D. Radford, R.G. Rigg, Hyd. Proc., November (1970) 187.